phys. stat. sol. (b) **217**, 63 (2000)

Subject classification: 71.15.–m; 71.20.Ps; 71.55.Ht; 75.25.+z; 75.50.Ee; S9.11

The Periodic Hartree-Fock Method and Its Implementation in the CRYSTAL Code

R. DOVESI (a), R. ORLANDO (a), C. ROETTI (a), C. PISANI (a), and V.R. SAUNDERS (b)

(a) Dipartimento di Chimica IFM, Università di Torino, via Giuria 5, I-10125 Torino

(b) CLRC Laboratory, Daresbury, Warrington, Cheshire, WA4 4AD, U.K.

(Received August 10, 1999)

The present chapter discusses the Hartree-Fock (HF) method for periodic systems with reference to its implementation in the CRYSTAL program. The HF theory is shortly recalled in its Closed Shell (CS), Unrestricted (UHF) and Restricted open shell (RHF) variants; its extension to periodic systems is illustrated. The general features of CRYSTAL, the periodic ab initio linear combination of atomic orbitals (LCAO) program, able to solve the CS, RHF and UHF, as well as Kohn-Sham equations, are presented. Three examples illustrate the capabilities of the CRYSTAL code and the quality of the HF results in comparison with those obtained with the Local Density Approximation using the same code and basis set: NiO in its ferro-magnetic and anti-ferromagnetic structure, trapped electron holes in doped alkaline earth oxides, and F-centres in LiF.

1. Introduction

For three decades the Hartree-Fock (HF) method has been the most popular scheme for the investigation of the electronic structure of atoms, molecules and clusters, either as such or as a well defined starting point for more sophisticated techniques. Since the beginning of the seventies, theoretical chemists have succeeded in developing powerful, general purpose, universally adopted HF-based ab initio computer programs [1]. The features of the most successful codes are essentially the same: the linearized HF-Roothaan equations are solved by using a few localized functions per atom (usually indicated as "atomic orbitals", AOs) as a basis set; in turn, the AOs are expressed as linear combinations of Gaussian type functions (GTF) with appropriate exponents and "contraction" coefficients; after obtaining the molecular orbitals (MO), eigenvectors of the Fock matrix, through a self consistent field (SCF) procedure, the correlation correction to the ground state wave function and properties, and the description of excited states are usually performed by means of configuration interaction (CI) or perturbation techniques. A posteriori, theoretical quantum chemistry appears to have followed quite a linear development from the original formulation of the HF equations by Fock, Hartree and Slater [2, 3], their linearized expression by Roothaan and Hall [4, 5], Boys' anticipation of present day techniques [6 to 8], to the full implementation of efficient computational tools. This has required a huge effort and ingenuity as concerns the definition of standard and well assessed basis sets [9, 10], the development of powerful *analytic* integration techniques [11 to 13], the efficient treatment of hundreds of thousand configurations in CI calculations [14], the new ideas for the

solution of the correlation problem [15]. In parallel, a set of semi-empirical electronic structure theories have been developed which, starting from the HF equations, on the one hand drastically reduce the computational effort by disregarding or approximating most of the bielectronic integrals, on the other incorporate correlation effects by way of largely intuitive approximations. A survey of these methods can be found in Ref. [16].

Density Functional Theory [17, 18] (DFT), that had played for long time a minor role in molecular quantum chemistry, has become more and more popular in the last years, and DFT related computational schemes are now available in standard ab initio molecular codes [19].

The situation in computational solid state physics and chemistry is quite different from the one sketched above for molecular quantum chemistry.

A great variety of formal schemes, computational methods and techniques are adopted for the determination of the electronic structure of crystalline compounds; the various proposals (many of them are presented in this book) differ in many respects, including the basis set (numerical, plane waves, localized, mixed), solution techniques of the basic equations, selected Hamiltonian and all its ingredients. The relative merits and limits of the various proposals are difficult to assess at the moment, as many of the computer codes are not available to the scientific community and are often in rapid evolution. The main reason for this situation is that computational solid state physics is a relatively young science with respect to molecular quantum chemistry: ab initio methods appeared in the late seventies, and the first general, portable, publicly available code, CRYSTAL88 [20], was distributed only ten years ago; in solid state computational physics, it is just at the beginning that "filtering" process that in molecular quantum chemistry led, for example, to abandon Slater and lobe type orbitals [21], owing to the difficulties encountered in the analytic evaluation of many mono- and bielectronic integrals in the former case [22], and because of the poor numerical accuracy obtained for integrals involving high angular quantum number AOs with the latter basis type.

There are, however, two features that are common to most periodic computer programs:

a) the use of DFT based Hamiltonians, the only exception being the CRYSTAL [23, 24] code, that can solve both the HF and Kohn-Sham (KS) equations;

b) the prevalent use of numerical rather than analytical techniques.

As a matter of fact, the HF approach has never been very popular among solid state physicists, for many reasons; probably the most important two are:

– HF performs poorly for the electron gas, the simplest of all periodic systems; it has very often been assumed that this remains true (or possibly gets worse) for most properties of real solids.

– The non-local exchange term makes the HF equations more difficult to solve than the KS ones, where the exchange–correlation potential $\mu_{xc}(\mathbf{r}; [\varrho])$ is simply a multiplicative operator, no matter how complicated its determination.

Early attempts at formulating and implementing HF computational schemes for periodic systems had scant success, in spite of the high quality and generality of some of them [25 to 30]. Only in recent years has it become possible to formulate a fair judgement about the usefulness of the HF approach in solid state physics, since the advent of

powerful computers and of general purpose computational schemes [20, 23, 24, 31], which have allowed us to assess its performance for a variety of systems [32].

In this chapter we will recall the general features of the HF scheme, both in its formulation for closed and open shell systems, and its generalization to periodic compounds when a local basis is used. Explicitly referring to the implementation in the CRYSTAL program, we will shortly recall some of the most critical points of this implementation and show that all the relevant interactions are evaluated analytically. This requires a much bigger implementation effort, but ensures a very high numerical accuracy, that is necessary in many cases, for example, in chemical reactions [33, 34] and in the study of magnetic interactions [35 to 37], that are of the order of a fraction of a kJ/mol.

The chapter ends up with a few applications; all of them refer to cases in which paramagnetic species are involved; the UHF results will be compared with DFT data obtained with the same basis set.

2. Hartree-Fock Theory

The non-relativistic Born-Oppenheimer Hamiltonian operator for a finite cluster of N nuclei and m electrons has the form

$$\widehat{H} = -\tfrac{1}{2}\sum_{i=1}^{m} \nabla_i^2 - \sum_{i=1}^{m}\sum_{A=1}^{N} \frac{Z_A}{|\mathbf{r}_i - \mathbf{A}|} + \sum_{i=1}^{m}\sum_{j=1}^{i-1} |\mathbf{r}_i - \mathbf{r}_j|^{-1} + \mathcal{N}\,, \tag{1}$$

where Z_j denotes the atomic number of the j-th nucleus, and

$$\mathcal{N} = \sum_{A=1}^{N}\sum_{B=1}^{A-1} \frac{Z_A Z_B}{|\mathbf{A} - \mathbf{B}|} \tag{2}$$

is the nuclear repulsion energy. In the above equations atomic units are used. The Hamiltonian of Eq. (1) is parametrically dependent only on the nuclear coordinates, **A**. A trial HF wave function is a single determinantal function constructed by antisymmetrizing a Hartree product of m single particle spin orbitals,

$$\Psi = \widehat{A}\left[\prod_{i}^{m} (\psi_i(\mathbf{r}_i)\,\chi(i))\right], \tag{3}$$

(ψ and χ denote the orbital and spin functions, respectively; $\widehat{A}$ is the antisymmetrizing operator) and is obviously an approximate solution to Eq. (1). The HF electronic wave function is variationally *the best* among these single determinantal functions.

2.1 Restricted closed shell (CS) theory for molecular systems

In the CS [5, 6] theory, the same molecular orbital (MO) is used to define both an α- and a β-spin orbital; the wave function is then constructed from $m_\mathrm{d}(m_\mathrm{d} = m/2)$ doubly occupied orbitals

$$\Psi_\mathrm{CS} = \widehat{A}\left[\prod_{i}^{m_\mathrm{d}} (\psi_i(\mathbf{r}_{2i-1}\alpha)\;\psi_i(\mathbf{r}_{2i}\beta)\right]. \tag{4}$$

The expectation value of the Hamiltonian with respect to the trial HF wave function, an approximation to the total electronic energy, takes the form

$$
\begin{aligned}
E_{\mathrm{CS}} &= \langle \Psi_{\mathrm{CS}} |\, H \,| \Psi_{\mathrm{CS}} \rangle \\
&= 2 \sum_{i}^{m_{\mathrm{d}}} \int \mathrm{d}\mathbf{r}\, \{ \psi_i^*(\mathbf{r})\, [-\nabla^2/2 + v(\mathbf{r})]\, \psi_i(\mathbf{r}) \} \\
&\quad + \sum_{ij}^{m_{\mathrm{d}}} \int \mathrm{d}\mathbf{r}\, \mathrm{d}\mathbf{r}'\, [\psi_i^*(\mathbf{r})\, \psi_i(\mathbf{r})]\, [\psi_j^*(\mathbf{r}')\, \psi_j(\mathbf{r}')]/|\mathbf{r} - \mathbf{r}'| \\
&\quad - \tfrac{1}{2} \sum_{ij}^{m_{\mathrm{d}}} \int \mathrm{d}\mathbf{r}\, \mathrm{d}\mathbf{r}'\, [\psi_i^*(\mathbf{r})\, \psi_j(\mathbf{r})]\, [\psi_j^*(\mathbf{r}')\, \psi_i(\mathbf{r}')]/|\mathbf{r} - \mathbf{r}'| \,. \qquad (5)
\end{aligned}
$$

The above total energy expression is to be minimized with respect to variations in the orbitals, subject to the orthonormality constraint among the orbitals,

$$
\int \psi_i^*(\mathbf{r})\, \psi_j(\mathbf{r})\, \mathrm{d}\mathbf{r} = \delta_{ij} \,. \qquad (6)
$$

The resulting HF equation takes the form ($\widehat{f}$ stands for the Fock Hamiltonian)

$$
\begin{aligned}
\widehat{f}\, \psi_i(\mathbf{r}) &\equiv [-(1/2)\, \nabla^2 + v(\mathbf{r}) + \int \mathrm{d}\mathbf{r}'\, \varrho(\mathbf{r}')/|\mathbf{r} - \mathbf{r}'|]\, \psi_i(\mathbf{r}) \\
&\quad - \sum_{j}^{m_{\mathrm{d}}} \int \mathrm{d}\mathbf{r}'\, [\psi_j^*(\mathbf{r}')\, \psi_i(\mathbf{r}')]/|\mathbf{r} - \mathbf{r}'|]\, \psi_j(\mathbf{r}) \\
&= \varepsilon_i \psi_i(\mathbf{r}) \,, \qquad (7)
\end{aligned}
$$

where the electron charge density $\varrho(\mathbf{r})$ is defined in terms of the $\psi_j(\mathbf{r})$ functions as follows:

$$
\varrho(\mathbf{r}) = 2 \sum_{j}^{m_{\mathrm{d}}} |\psi_j(\mathbf{r})|^2 \qquad (8)
$$

and the factor two is due to the double occupation of the orbitals. The first three terms (kinetic, nuclear attraction, inter-electronic Coulomb repulsion) in Eq. (7) coincide with the corresponding ones which appear in the KS equations of DFT. The last term represents the "exact" non-local exchange operator, that in the KS equation is substituted by the effective exchange–correlation potential, $\mu_{\mathrm{xc}}(\mathbf{r}; [\varrho])$. Like the KS equations, the HF equations must be solved through a Self-Consistent (SC) procedure, since both the Coulomb and the exchange operators depend on the set of functions, $\psi_i(\mathbf{r})$.

If we express the molecular orbitals, ψ_i, as linear combinations of n_{b} local (and real) functions φ_μ (AOs, the basis set),

$$
\psi_i = \sum_{\mu}^{n_{\mathrm{b}}} c_{\mu i} \varphi_\mu \,. \qquad (9)
$$

Eq. (7) transforms into the following matrix equation:

$$
FC = SCE \,, \qquad (10)
$$

where F and S are the Fock and the overlap matrices, C and E the eigenvectors and eigenvalues. The expression of the various contributions to F is given below

$$
F_{\mu\nu} = T_{\mu\nu} + Z_{\mu\nu} + B_{\mu\nu} + X_{\mu\nu} \,, \qquad (11)
$$

where

$$
T_{\mu\nu} = -\tfrac{1}{2} \int \varphi_\mu(\mathbf{r})\, \nabla_{\mathbf{r}}^2 \varphi_\nu(\mathbf{r})\, \mathrm{d}\mathbf{r} \,, \qquad (12)
$$

$$Z_{\mu\nu} = \sum_{A=1}^{N} \int \varphi_\mu(\mathbf{r}) \, \frac{Z_A}{|\mathbf{r} - \mathbf{A}|} \, \varphi_\nu(\mathbf{r}) \, \mathrm{d}\mathbf{r} \,, \tag{13}$$

$$B_{\mu\nu} = \sum_{\lambda\varrho}^{n_\mathrm{b}} P_{\lambda\varrho} \, (\mu\nu \mid \lambda\varrho) \,, \tag{14}$$

$$X_{\mu\nu} = -\tfrac{1}{2} \sum_{\lambda\varrho}^{n_\mathrm{b}} P_{\lambda\varrho} \, (\mu\lambda \mid \nu\varrho) \,, \tag{15}$$

and

$$(\mu\nu \mid \lambda\varrho) = \int\int \varphi_\mu(\mathbf{r}) \, \varphi_\nu(\mathbf{r}) \, |\mathbf{r} - \mathbf{r}'|^{-1} \, \varphi_\lambda(\mathbf{r}') \, \varphi_\varrho(\mathbf{r}') \, \mathrm{d}\mathbf{r} \, \mathrm{d}\mathbf{r}' \tag{16}$$

$$P_{\mu\nu} = 2 \sum_i c^*_{\mu i} c_{\nu i} \,, \tag{17}$$

$$E_\mathrm{CS} = \tfrac{1}{2} \sum_{\mu\nu}^{n_\mathrm{b}} P_{\mu\nu} (F_{\mu\nu} + T_{\mu\nu} + Z_{\mu\nu}) \,. \tag{18}$$

2.2 Unrestricted (UHF) and restricted Half-closed-shell (RHF) Hartree-Fock theories

For the description of systems containing unpaired electrons (such as atoms, molecules with an odd number of electrons, radicals) a single determinant is not, in the most general case, an appropriate wave function. In order to get the correct spin eigenfunction of these systems, it is necessary to choose a linear combination of Slater determinants (whereas, in closed shell systems, a single determinant always gives the appropriate spin eigenfunction). The UHF and RHF approximations permit, however, to describe open shell systems while maintaining the simplicity of the single determinant approximation.

In the RHF approximation [38, 39] the wave function is a single determinant constructed from m_d doubly occupied orbitals (the same MO being used to define both an α- and a β-spin orbital), and a further m_s singly occupied MOs whose spins are all aligned in parallel and which constitute the half-closed-shell. We therefore have $m = 2m_\mathrm{d} + m_\mathrm{s}$.

In the UHF theory [40] the spin orbitals are taken to be of the form

$$\psi(\mathbf{x}) = \psi^\alpha(\mathbf{r}) \, \alpha(\sigma) \quad \text{or} \quad \psi^\beta(\mathbf{r}) \, \beta(\sigma) \,. \tag{19}$$

The double occupancy constraint allows the RHF approach to obtain solutions that are eigenfunctions of the spin operator, $\widehat{S}^2$, whereas UHF solutions are formed by a mixture of spin states (both are eigenfunctions of $\widehat{S}_z$). The greater variational freedom allows the UHF method to produce wave functions that are energetically more stable than the corresponding RHF ones; another advantage of the UHF method is that it allows solutions with locally negative spin density (i.e. anti-ferromagnetic systems), a feature that RHF solutions cannot possess.

The molecular orbital diagram for the UHF and RHF cases is shown in Fig. 1. We refer to the original papers quoted above, or to molecular quantum mechanics textbooks for the definition of the expressions equivalent to Eqs. (10) to (18) in the UHF and RHF cases.

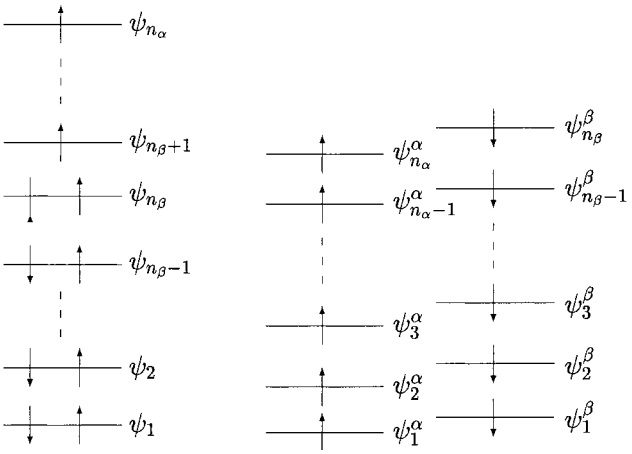

Fig. 1. Molecular orbital diagram for the Restricted Open Shell (RHF, left) and the Unrestricted (UHF, right) Hartree-Fock methods

3. Hartree-Fock Theory for Periodic Systems; the CRYSTAL Program

At first sight, the reformulation of the HF-Roothaan equations (Eqs. (10) to (18)) sketched above, to make them suitable for crystalline systems is a relatively easy task, and has been proposed more than thirty years ago by various authors [26 to 28]. Starting from a set of localized functions in the unit reference cell of the crystal, $\varphi_\mu(\mathbf{r})$ $(\mu = 1, ..., p)$, it is possible to build Bloch functions (BF),

$$\phi_\mu(\mathbf{k}, \mathbf{r}) = \sum_{\mathbf{G}} \exp\,(i\mathbf{k} \cdot \mathbf{G})\; \varphi_\mu(\mathbf{r} - \mathbf{G})\,, \tag{20}$$

where the sum is extended to all **G** vectors of the direct lattice, while **k** is a general vector in the first Brillouin zone (BZ). The resulting set of equations is in one-to-one correspondence with Eqs. (10) to (18).

3.1 The formal equations for closed shell systems

In the basis of the Bloch functions, the Fock matrix becomes

$$F_{\mu\nu}(\mathbf{k}) = \sum_{\mathbf{G}} \mathrm{e}^{i\mathbf{k}\mathbf{G}}\; F_{\mu\nu}(\mathbf{G})\,, \tag{21}$$

where $F_{\mu\nu}(\mathbf{G})$ is the matrix element of the Fock operator between the μ-th AO located in the *zero* cell and the ν-th AO located in the **G** cell. The row index can be limited to the *zero* cell for translational symmetry. Matrices represented in the Bloch basis (or in "**k** space") take a block diagonal form, as Bloch functions are bases for the Irreducible Representations (IR) of the Translation Group (TG); each block has the dimensions of the AO basis in the unit cell, n_b,

$$F(\mathbf{k})\; C(\mathbf{k}) = S(\mathbf{k})\; C(\mathbf{k})\; E(\mathbf{k})\,. \tag{22}$$

In principle the above equation should be solved for all the (infinite) **k** points of the Brillouin zone; fortunately, only a finite and usually small subset of these blocks, corresponding to a suitable sampling of **k** points, needs to be diagonalized, because interpo-

lation techniques can be used for eigenvalues and eigenvectors throughout the first Brillouin zone.

$$F_{\mu\nu}(\mathbf{G}) = \mathbf{T}_{\mu\nu}(\mathbf{G}) + \mathbf{Z}_{\mu\nu}(\mathbf{G}) + \mathbf{B}_{\mu\nu}(\mathbf{G}) + \mathbf{X}_{\mu\nu}(\mathbf{G})\,, \tag{23}$$

$$T_{\mu\nu}(\mathbf{G}) = \int \varphi_\mu(\mathbf{r})\ \nabla^2_{\mathbf{r}} \varphi_\nu(\mathbf{r}-\mathbf{G})\ \mathrm{d}\mathbf{r}\,, \tag{24}$$

$$Z_{\mu\nu}(\mathbf{G}) = \sum_{A=1}^{\mathrm{N}} \sum_{\mathbf{M}} \int \varphi_\mu(\mathbf{r})\ \frac{Z_A}{|\mathbf{r}-\mathbf{A}-\mathbf{M}|}\ \varphi_\nu(\mathbf{r}-\mathbf{G})\ \mathrm{d}\mathbf{r}\,, \tag{25}$$

$$B_{\mu\nu}(\mathbf{G}) = \sum_{\lambda\varrho}^{\mathbf{n}_\mathrm{b}} \sum_{\mathbf{G}'} \mathbf{P}_{\lambda\varrho}(\mathbf{G}') \sum_{\mathbf{M}} (\mu\mathbf{0}\nu\mathbf{G} \mid \lambda\mathbf{M}\varrho(\mathbf{M}+\mathbf{G}'))\,, \tag{26}$$

$$X_{\mu\nu}(\mathbf{G}) = -\tfrac{1}{2} \sum_{\lambda\varrho}^{n_\mathrm{b}} \sum_{\mathbf{G}'} P_{\lambda\varrho}(\mathbf{G}') \sum_{\mathbf{M}} (\mu\mathbf{0}\lambda\mathbf{M} \mid \nu\mathbf{G}\varrho(\mathbf{M}+\mathbf{G}'))\,, \tag{27}$$

$$P_{\lambda\varrho}(\mathbf{G}') = 2 \int \mathrm{d}\mathbf{k}\ \mathrm{e}^{i\mathbf{k}\mathbf{G}'} \sum_{j}^{n_\mathrm{b}} c^*_{\lambda j}(\mathbf{k})\ c_{\varrho j}(\mathbf{k})\ \theta(\epsilon_\mathrm{F} - \epsilon_j(\mathbf{k}))\,, \tag{28}$$

$$E_\mathrm{CS} = \tfrac{1}{2} \sum_{\mu\nu}^{n_\mathrm{b}} \sum_{\mathbf{G}} P_{\mu\nu}(\mathbf{G})\ (\mathbf{F}_{\mu\nu}(\mathbf{G}) + \mathbf{T}_{\mu\nu}(\mathbf{G}) + \mathbf{Z}_{\mu\nu}(\mathbf{G}))\,, \tag{29}$$

where ϵ_F is the Fermi energy, the integration in Eq. (28) extends to the first Brillouin zone, and $c_j(\mathbf{k})$ and $\epsilon_j(\mathbf{k})$ are eigenvectors and eigenvalues of the $F(\mathbf{k})$ matrix.

The above equations, as such, are useless, because the $\mathbf{G}$, $\mathbf{G}'$ and $\mathbf{M}$ summations extend to the infinite set of translation vectors; a strategy must then be specified for the treatment of the infinite Coulomb and exchange series, as well as for the substitution of the integral that appears in Eq. (28) with a weighted sum extended to a finite set of $\mathbf{k}$ points. An accurate and efficient solution to these problems has been implemented in the CRYSTAL code [23, 24, 31, 32]. Some of the features of CRYSTAL will be summarized in the next section. Before moving to these technical aspects, we want however to spend a few more words on the periodic UHF method, as all the applications discussed in the last section concern paramagnetic species.

3.2 The UHF equations

In the UHF case, two sets of matrix equations must be solved self-consistently, for α and β electrons,

$$F^\alpha(\mathbf{k})\ C^\alpha(\mathbf{k}) = S(\mathbf{k})\ C^\alpha(\mathbf{k})\ E^\alpha(\mathbf{k})\,, \tag{30}$$

$$F^\beta(\mathbf{k})\ C^\beta(\mathbf{k}) = S(\mathbf{k})\ C^\beta(\mathbf{k})\ E^\beta(\mathbf{k})\,, \tag{31}$$

where the $F^\alpha(\mathbf{k})$, $F^\beta(\mathbf{k})$ and $S(\mathbf{k})$ matrices are obtained by Fourier transform from the corresponding "direct space" equivalent quantities as in Eq. (21).

We now define the *total density* (P) and *spin density* (P^spin) matrices,

$$P(\mathbf{G}) = P^\alpha(\mathbf{G}) + P^\beta(\mathbf{G})\,, \tag{32}$$

$$P^\mathrm{spin}(\mathbf{G}) = P^\alpha(\mathbf{G}) - P^\beta(\mathbf{G})\,, \tag{33}$$

where $P^\alpha(\mathbf{G})$ and $P^\beta(\mathbf{G})$ are obtained as in Eq. (28) by using the α and β eigenvectors obtained from Eq. (30) and (31), respectively.

The $F^{\alpha}(\mathbf{G})$ and $F^{\beta}(\mathbf{G})$ matrices are defined as follows:

$$F^{\alpha}_{\mu\nu}(\mathbf{G}) = F_{\mu\nu}(\mathbf{G}) - X^{\text{spin}}_{\mu\nu}(\mathbf{G}) , \tag{34}$$

$$F^{\beta}_{\mu\nu}(\mathbf{G}) = F_{\mu\nu}(\mathbf{G}) + X^{\text{spin}}_{\mu\nu}(\mathbf{G}) . \tag{35}$$

The $F(\mathbf{G})$ matrix is defined as in Eq. (23), where the total density matrix $P(\mathbf{G})$ defined in Eq. (32) is used in the Coulomb and exchange terms; $X^{\text{spin}}_{\mu\nu}(\mathbf{G})$ is defined as $X_{\mu\nu}(\mathbf{G})$ in Eq. (27), where however the spin density matrix $P^{\text{spin}}(\mathbf{G})$ is used instead of the total density matrix $P(\mathbf{G})$.

4. The Implementation of the Periodic HF Equations in the CRYSTAL Program

CRYSTAL is an ab initio periodic computer program implemented by the Group of Theoretical Chemistry of the University of Torino (Italy) in collaboration with the Computational Group at the Daresbury Laboratory (UK). The first version was distributed in 1988 [20], and for about ten years it has been the only public general-purpose ab initio periodic computer program; three improved versions of CRYSTAL were subsequently released; [23, 41, 42] (the last one is in distribution since the beginning of 1999). More than 200 copies of both the '92 and '95 versions have been distributed over the world.

4.1 The general features

We summarize here the main features of the CRYSTAL98 program:

1. It is a "direct space" program, in the sense that all the relevant quantities (mono- and bi-electronic integrals, overlap and Fock matrices, see Eqs. (23) to (29)), are computed in the configuration space. Just before the diagonalization step the Fock matrix is

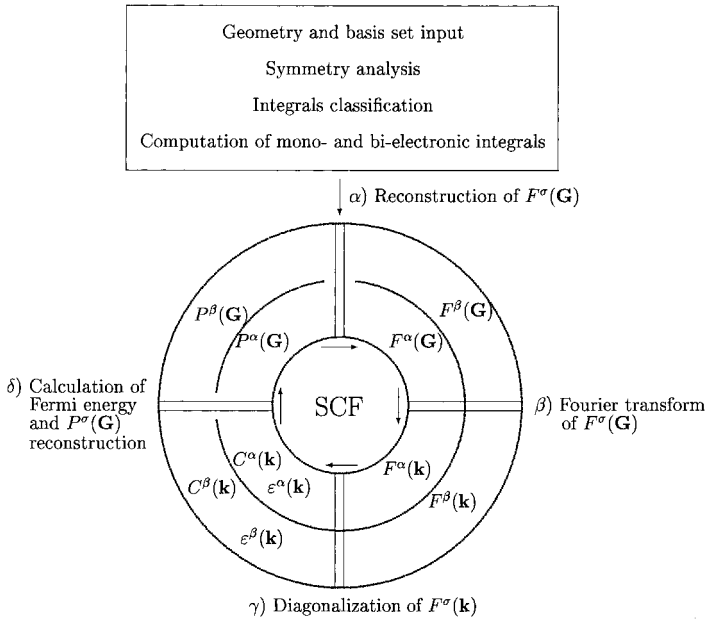

Fig. 2. Scheme of the implementation of the UHF method in CRYSTAL

Fourier transformed to reciprocal space (Bloch functions basis; see Eq. (21)), then the eigenvalues and eigenvectors of the $F(\mathbf{k})$ matrices are combined to generate the "direct space" density matrix for the next SCF cycle (Eq. (28)).

2. In its most recent version, CRYSTAL can solve the HF as well as the KS equations; as regards the latter, the most popular *local* and *non local* functionals are available, as well as *hybrid* schemes, such as the so called B3-LYP, which combines the HF exchange term with the Becke [43] and Lee-Yang-Parr [44] functionals according to the formula proposed by Becke [45]. As regards the former, the CS, RHF and UHF options are available. Schemes are also available, that permit to correct the HF total energy by estimating the correlation energy *a posteriori*, integrating a correlation-only functional of the HF charge density. This latter scheme has been shown to provide accurate binding energies for a large family of compounds [32].

The general structures of the program is illustrated in Fig. 2, for the case of the UHF path. The scheme shows that the most relevant quantities (Fock and density matrices, eigenvalues and eigenvectors) are duplicated, so that it is possible to differentiate α from β orbitals. The two sections of the code, corresponding to α and β electrons, are independent until the Fermi energy calculation and Fock matrix reconstruction. It is then possible to force the system into a state with a particular S_z value, by imposing the desired $m_\alpha - m_\beta$ value when the crystalline monoelectronic energy levels are populated at each cycle of the SC step.

Many steps of the calculation are common to the HF and DFT options (for example the treatment of the Coulomb series, which are evaluated analytically, as discussed below); the main difference concerns, obviously, the exchange (and correlation) contribution to the Hamiltonian matrix and total energy: in the HF case the exchange bielectronic integrals are evaluated analytically, and the exchange series is truncated after a certain number of terms, as discussed below. In the DFT calculations [46], the exchange–correlation potential is expanded in an auxiliary basis set of GTF, with even tempered exponents. At each SCF iteration the auxiliary basis set is fitted to the actual analytic form of the exchange–correlation potential, which changes with the evolving charge density. For numerical integration, the atomic partition method proposed by Becke [47] has been adopted, combined with the Gauss-Legendre (radial) and Lebedev (angular) quadratures.

3. It can treat systems periodic in 0 (molecules), 1 (polymers), 2 (slabs) and 3 (crystals) directions with similar accuracy; this permits the evaluation of energy differences such as bulk-minus-molecule (lattice energy of a molecular crystal), bulk-minus-slab (surface energy), bulk-minus-chain (inter-chain interactions) with high accuracy, as well as energy differences between crystals with different cell size, shape, and number of atoms.

4. All the crystalline space, layer and rod groups are available, simply by specifying the label of the group according to the international crystallographic notations.

5. Several geometrical options are available, which permit an easy manipulation of the cell (creating defects, distorting the cell, building supercells, cutting slabs from the bulk, extracting molecules from the bulk, and so on).

4.2 The treatment of the infinite Coulomb and exchange series

As anticipated, the problem with the formal periodic equations (22) to (29), is that they contain three infinite summations ($\mathbf{G}$, $\mathbf{G}'$ and $\mathbf{M}$), that extend to all lattice vectors. We

refer to previous papers for an exhaustive presentation of the strategy adopted in CRYSTAL for the treatment of the Coulomb [31, 48] and exchange [24] series. Here we summarize the main ideas:

– *The general strategy is to evaluate the integrals analytically, whenever possible.* The core of the integral package in the CRYSTAL code derives from the GAUSSIAN70 [1] and ATMOL [49] integral packages; both have been heavily modified and generalized for many reasons, and new parts have been added. As regards the latter point, the following new kinds of integrals are required for the construction of the Fock operator:

a) multipolar integrals of a product of two GTFs;

b) bipolar expansions of two interacting charge distributions represented by a product of two AOs each;

c) interaction of a charge distribution $\varrho_{\mu\nu}$ with the infinite array of point charges and higher multipoles of a charge distribution. These integrals are evaluated analytically using Ewald type techniques through a combination of recursion relations involving Hermite polynomials and spherical harmonics, so that all the integrals can be obtained from the generalized error functions, as for molecular integrals [31, 48].

Specific routines are available for periodicity in one, two and three dimensions (see Refs. [31, 50]).

– *The overlap between two GTFs decays exponentially with distance.* This property can be exploited for the truncation of the **G** and **G**′ sums in the Coulomb term (see Eq. (26) and (29)) and for two of the exchange summations (Eq. (28)). In a similar way the overlap, kinetic, nuclear attraction integrals can be reduced to the consideration of a finite number of neighbours of the reference cell. The screening criteria are applied both to the contracted AOs, and to the single Gaussians of a contraction. An efficient sorting of the **G** vectors and evaluation of the overlap between shell couples allow a rapid selection of the integrals to be computed.

– *The density matrix elements decay with distance between the involved functions.* In a localized basis set, the elements of the density matrix of an insulator decay exponentially with the distance between the two centres, the larger the gap the faster the decay. Density matrix in direct space decays to zero with distance for conductors, too, but much more slowly [24, 51].

This behaviour is exploited for an efficient truncation of the exchange series in the Fock matrix (Eq. (27)) and total energy (Eq. (29)) expressions. The two above equations show that the **M** summation is limited by the exponential decay of the product $\varphi_\mu\varphi_\lambda$ and for a similar reason the $|\mathbf{G} - \mathbf{M} - \mathbf{G}'|$ distance cannot be too large. These two conditions imply that the **G** and **G**′ vectors cannot be very different, although their moduli could be large. However, the exponential decay of the density matrix permits us to disregard integrals involving **G** and **G**′ vectors with large moduli. The exchange series are then truncated according to these criteria. Long range effects are not taken into account, as they are negligible. Exchange bielectronic integrals are evaluated as such or through a *bipolar expansion* (see below), when the two charge distributions do not overlap.

– *The multipolar expansion and the Ewald method for the Coulomb series.* Let us define a partition of the cell charge distribution, for example in terms of Mulliken atomic charges ϱ_A,

$$\varrho(\mathbf{r}) = \sum_A \sum_{\mathbf{M}} \varrho_A(\mathbf{r} - \mathbf{A} - \mathbf{M}) \,, \tag{36}$$

where

$$\varrho_A(\mathbf{r}-\mathbf{A}) = \sum_{\lambda\in A}\sum_{\varrho}\sum_{\mathbf{G}'} P_{\lambda\varrho}(\mathbf{G}')\ \varphi_\lambda(\mathbf{r})\ \varphi_\varrho(\mathbf{r}-\mathbf{G}') - Z_A\ \delta(\mathbf{r}-\mathbf{A}) \tag{37}$$

is translationally invariant and the last term is the nuclear charge contribution. The sum of the electron–electron and electron–nuclei contributions to the Fock matrix, $R_{\mu\nu}(\mathbf{G}) = B_{\mu\nu}(\mathbf{G}) + Z_{\mu\nu}(\mathbf{G})$ (Eq. (25) and (26)), can then be written as

$$R_{\mu\nu}(\mathbf{G}) = \sum_A \sum_{\mathbf{M}} \iint \varrho_{\mu\nu}(\mathbf{r}_1-\mathbf{G})\ |\mathbf{r}_1-\mathbf{r}_2|^{-1}\ \varrho_A(\mathbf{r}_2-\mathbf{A}-\mathbf{M})\ \mathrm{d}\mathbf{r}_1\ \mathrm{d}\mathbf{r}_2 \tag{38}$$

with

$$\varrho_{\mu\nu}(\mathbf{r}_1-\mathbf{G}) = \varphi_\mu(\mathbf{r}_1)\ \varphi_\nu(\mathbf{r}_1-\mathbf{G})\,. \tag{39}$$

If the charge distributions ϱ_A and $\varrho_{\mu\nu}$ do not overlap for any $\mathbf{M}$, Eq. (38) can be written as

$$R_{\mu\nu}(\mathbf{G}) = \sum_A \sum_{\ell m} \left(\sum_{\mathbf{M}} \gamma_{\ell m}(A)\ \Phi_{\mu\nu\ell m}(\mathbf{G},\mathbf{A}+\mathbf{M})\right), \tag{40}$$

so that $R_{\mu\nu}$ is expressed in terms of the multipole moments of ϱ_A ($N_{\ell m}$ is a normalization factor),

$$\gamma_{\ell m}(A) = \int \varrho_A(\mathbf{r}_2-\mathbf{A})\ N_{\ell m} X_{\ell m}(\mathbf{r}_2-\mathbf{A})\ \mathrm{d}\mathbf{r}_2 \tag{41}$$

and of the field integrals

$$\Phi_{\mu\nu\ell m}(\mathbf{G},\mathbf{A}+\mathbf{M}) = \int \varphi_\mu(\mathbf{r}_1)\ \varphi_\nu(\mathbf{r}_1-\mathbf{G})\ X_{\ell m}(\mathbf{r}_1-\mathbf{A}-\mathbf{M})\ |\mathbf{r}_1-\mathbf{A}-\mathbf{M}|^{-2\ell-1}\ \mathrm{d}\mathbf{r}_1\,. \tag{42}$$

where $X_{\ell m}$ is a real solid spherical harmonic.

The infinite $\mathbf{M}$ summation can be performed by using the Ewald technique, which reduces it to a finite number of new integrals, that can be evaluated analytically [31]. The main advantage of Eq. (38), with respect to Eq. (25) and (26), is that a large number of terms (typically, more than 1000 for a packed system like MgO with a double-ζ basis set) are summed up (Eq. (37)) and treated at the same time with a corresponding saving factor in computational effort. If $\varrho_{\mu\nu}$ and ϱ_A do overlap for some $\mathbf{M}$ vectors close to the origin (let us call this set $\mathbf{M}_B$), the same Ewald technique is used. A correction is however applied, consisting in subtracting by direct summation the contribution from the $\mathbf{M}_B$ set in Eq. (40), and adding the corresponding contribution from Eq. (25) and (26). The resulting finite (possibly small) number of bielectronic Coulomb integrals and nuclear attraction integrals is then evaluated with standard techniques; it is, however, to note that a non negligible fraction of integrals corresponding to the $\mathbf{M}_B$ set can be approximated by a *bipolar expansion* of both charge distributions, because it may happen that, although ϱ_A is penetrating $\varrho_{\mu\nu}$, some of the contributions to ϱ_A are not, and can then be approximated (see Ref. [24], pp. 47 to 52).

– *Point symmetry.* A crucial point for the speed and accuracy of the calculation is the complete exploitation of symmetry. Point symmetry is exploited at various levels in CRYSTAL, both in the direct (AO) and reciprocal space (Bloch functions) representations.

As concerns the former aspect, two points are worth noting:

– The contributions to the Fock matrix $F_{\mu\nu}(\mathbf{G})$ are evaluated only for the set of indices $\mu\nu\mathbf{G}$ belonging to the *irreducible set*, i.e. to the minimal set necessary for the

generation of the complete matrix through the use of the point symmetry operations. The saving factor in CPU time and space requirements can be as large as h, the number of the symmetry operations in the point group. We remind here that *translational symmetry* has already been used for limiting the first index μ to the *zero* cell.

– Disk space requirements for the storage of the bielectronic integrals can be reduced, and the Fock matrix reconstruction at each step of the SCF stage can be accelerated by storing symmetrized sums of bielectronic integrals [24, 52].

Point symmetry is also exploited in those parts of the program which work in the Bloch function representation.

– In principle the Fock matrix must be diagonalized at all the **k** points of the first BZ. The eigenvalues are then used for the determination of the Fermi energy, and the eigenvectors for building the density matrix of the next cycle. It is, however, easily shown that the Fock matrix can be diagonalized only in the so-called *irreducible part* of the BZ (IBZ); the full set of eigenvectors can then be obtained by rotation of the eigenvectors of the IBZ.

– The set of operators that do not move a **k** point of the IBZ form the so-called little co-group [53] of the **k** point, and can be used to block-diagonalize the Fock matrix $F(\mathbf{k})$, by building symmetry adapted crystalline orbitals [54, 55]. This point is of minor importance when small unit cell systems are considered, as most of the **k** point have no symmetry at all; however, when large unit cell, highly symmetric systems are considered, the exploitation of this particular aspect of symmetry becomes essential, as the order of the little co-group of the few **k** points to be considered is quite high [56].

5. Examples of Applications

Applications of the HF-Crystalline Orbitals SCF method as implemented in the CRYSTAL program in many different areas have been performed by the present authors since 1980, when the first studies devoted to diamond and graphite were published [57, 58]; a complete list of our publications can be found at the web site *http://www.ch.unito.it/ifm/teorica/crystal.html*. Here, we concentrate on three applications involving uncoupled electrons, namely a transition metal oxide (NiO), a trapped hole in CaO bulk where a Li is substituted for a Ca atom, an F-centre (an electron trapped in an anion vacancy) in LiF. In all cases the UHF option has been used; for comparison, the calculations have been repeated at the spin polarized LDA (LSDA) level.

5.1 The electronic and magnetic properties of transition metal compounds: the case of NiO

NiO is a prototype compound in the family of transition metal oxides, and has been the subject of extensive theoretical investigations [59 to 64]. From an experimental point of view, these materials are classified as antiferromagnetic (AFM) ionic insulators. The band structures, obtained at the UHF and LSDA level (we refer to previous papers for the basis set description and other technical details [63, 64]), are reported in Fig. 3; the figure includes the valence bands, and three conducting bands: two of them are the empty (at the HF level) e_g levels, the third is an anti-bonding oxygen p band. The two band structures differ in many respects:

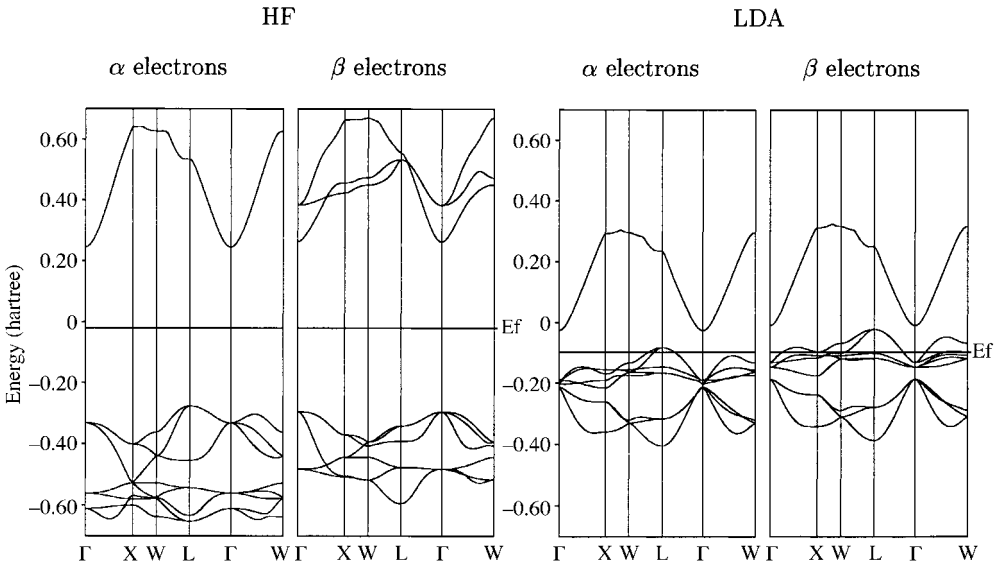

Fig. 3. HF and LDA NiO band structure; ferromagnetic solution

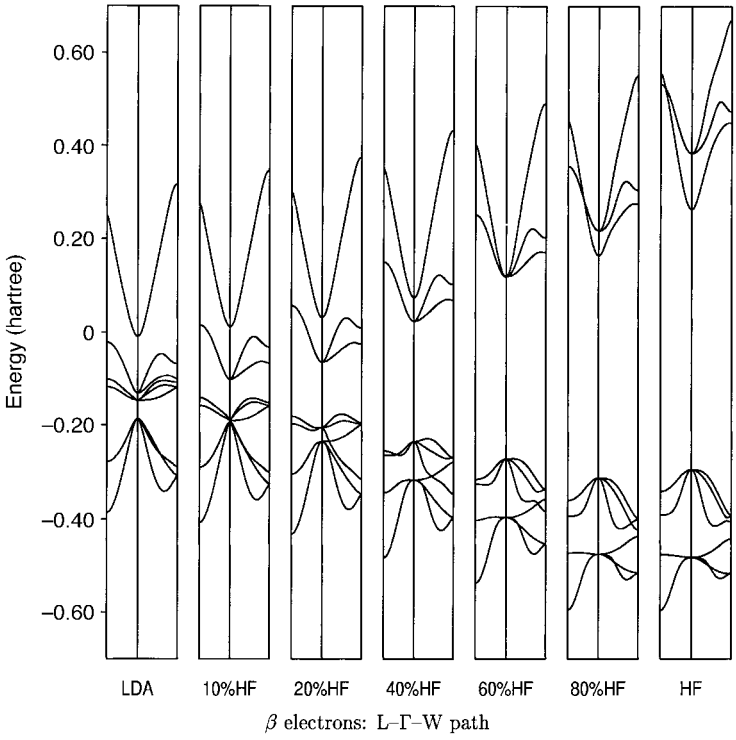

Fig. 4. NiO valence band structure obtained with Hamiltonians containing various mixing of the LDA and HF exchange potential. The three highest bands are empty, and correspond to the e_g empty states and to an antibonding p state. The LDA solution is metallic

(i) the HF solution presents a large gap, whereas the LDA solution is metallic; this behaviour is a direct consequence of the local character of the exchange term, as demonstrated by Fig. 4, where the results of various "hybrid" solutions, obtained by mixing in various percentages the HF and LDA exchange operator in the Hamiltonian, are reported.

(ii) The highest part of the valence band structure is mainly contributed by p oxygen states in the HF solution, whereas d states are predominant in the LDA solution.

As regards bulk properties, such as the lattice parameter, they are in line with previous experience: UHF overestimates (4.26 Å), whereas LSDA underestimates (4.10 Å) the experimental result (4.17 Å).

The electronic structure can be described in terms of Mulliken charges, as shown in Table 1. It turns out that the UHF solution is very ionic, with spin moments and net charges very close to the formal ones (+2 for Ni, eight electrons in the d shell), and a small and negative Ni–O bond population, indicating that the interaction between the two ions is essentially electrostatic, with a short range repulsion contribution. The ferromagnetic (FM) and AFM solutions are very similar, apart from the small spin polarization on the oxygen atom in the latter case; this is in qualitative agreement with the very small energy differences between the two solutions, that must imply very small differences in the wave function. The LSDA situation is quite different: the net charges are about 0.5 electrons smaller, and when a solution corresponding to two uncoupled electrons is imposed ($S_z = 1$), the spin polarization involves also the oxygen atom for about 0.5 electrons, whereas in the UHF case the oxygen spin polarization was much smaller (0.08 electrons). The LSDA FM and AFM solutions are quite different. The bond population, though small, is positive.

The very different spin polarization of the oxygen obtained with the two Hamiltonians in the FM state is also evident from the spin density map (Fig. 5, left), whereas it disappears, for symmetry reasons, in the AFM solution (Fig. 5, right). As the superexchange mechanism is mainly related to this oxygen polarization (see, for example, the discussion in Ref. [37]) it is clear why the LSDA Hamiltonian produces much higher energy differences between the FM and AFM states than UHF. The behaviour

Table 1

Net charges (q), spin moments (μ) and bond populations (q_{AB}) in the ferromagnetic and anti-ferromagnetic states of NiO evaluated according to a Mulliken partition. In the second row the number of electrons in the Ni d shell is reported. Units: electrons

		HF		LDA	
		FM	AF	FM	AF
q	Ni	+1.87	+1.86	+1.55	+1.50
	d_{Ni}	8.098	8.102	8.387	8.443
	O	−1.87	−1.86	−1.55	−1.50
μ	Ni	1.923	±1.913	1.556	±1.185
	d_{Ni}	1.919	±1.912	1.550	±1.185
	O	0.077	0	0.432	0
q_{AB}	Ni–O	−0.032	−0.032	+0.010	+0.018

of this quantity (ΔE) as a function of the lattice parameter in the UHF case is given in Fig. 6: it shows the rapid fall-down to zero (that is: the FM and AFM states have the same energy) for large Ni–O distance as a consequence of the exponential reduction of the short range inter-ionic repulsion; this behaviour has been documented experimentally in the case of the KMF_3 perovskites (M = Mn,Ni), in quite good agreement with the UHF results [37]. The LSDA ΔE value are much larger and show a different dependence on the Ni–O distance: it is ten times bigger at 3.80 Å, about

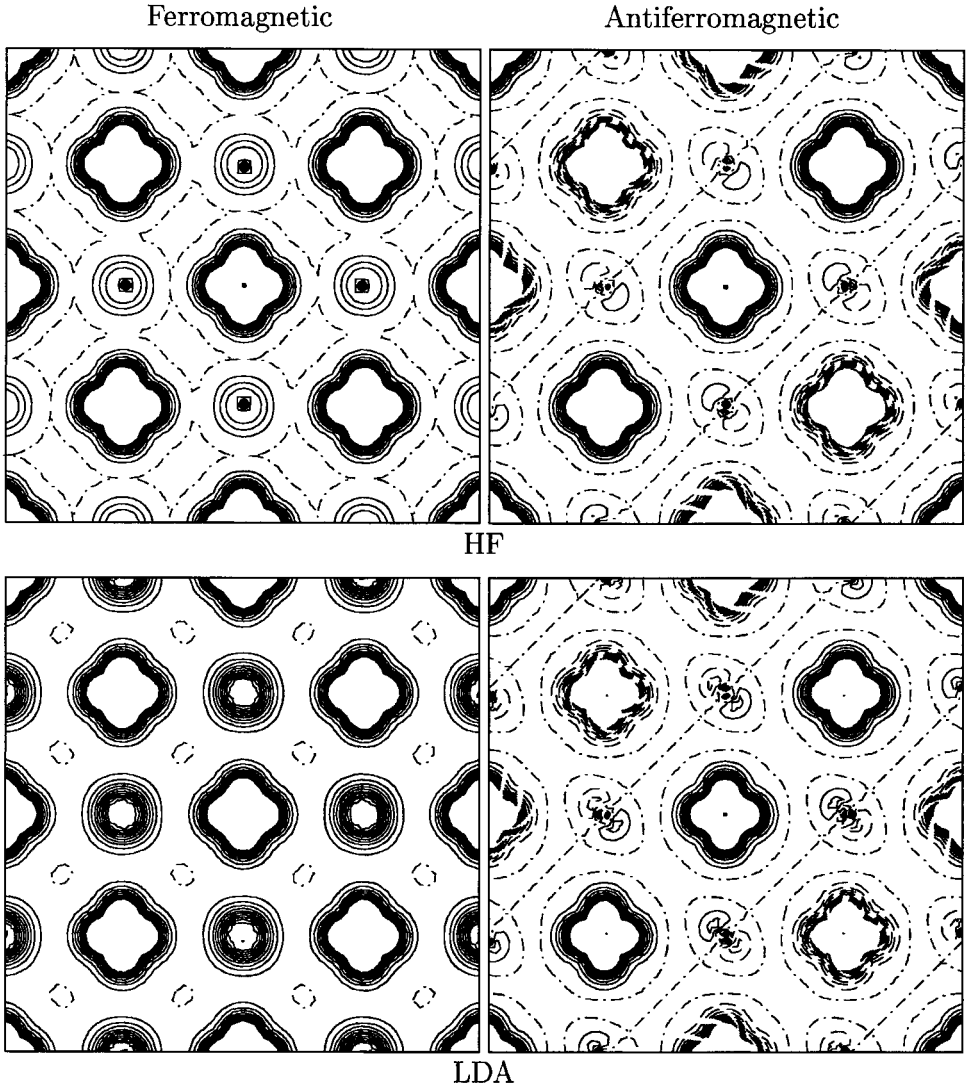

Fig. 5. HF and LDA spin density maps in the FM and AFM states; iso-density lines are drawn at intervals of 0.01 (Bohr)$^{-3}$; continuous, dashed and dash-dotted lines correspond to positive, negative and zero values, respectively

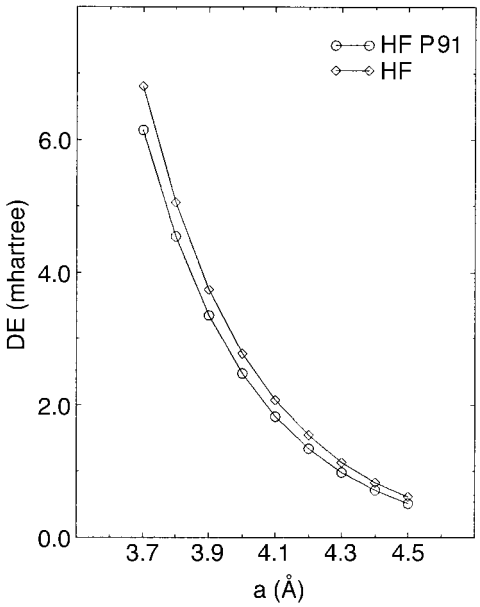

Fig. 6. Energy difference between the ferromagnetic and anti-ferromagnetic solutions for NiO as a function of lattice parameter. The two curves refer to HF energies (diamonds) and energies corrected with a correlation-only density functional (circles)

20 times bigger at the experimental geometry, 25 times bigger at 4.60 Å. In the cases where a direct comparison with experimental results is possible, as for the above mentioned KMF_3 perovskites, the UHF super-exchange constant extracted from ΔE turns out to be about one third of the corresponding experimental quantity [37].

5.2 Trapped electron holes in alkali doped alkaline earth oxides

Paramagnetic centres are formed when alkaline earth oxides, doped with alkali metal ions, are exposed to ionizing radiation at low temperature [65, 66]. EPR spectra give evidence of the formation of alkali metal trapped electron holes in oxides such as MgO, CaO and SrO [65 to 68], that are usually denoted as $[M]^0$. The interest in these materials is connected with two distinct applications: 1) their possible use as insulators in high radiation environments, as they can suppress radiation damage; 2) their catalytic activity in the formation of higher order hydrocarbons from methane, for possible exploitation in industrial processes [69, 70].

Electron Nuclear Double Resonance (ENDOR) spectroscopy has been applied to $[Li]^0$- and $[Na]^0$-doped isostructural oxides MgO, CaO and SrO for the accurate measurement of their hyperfine structure, which has provided useful information about the spin density distribution and geometry of the defects [71, 72].

The electronic structure and properties of trapped electron hole centres can also be investigated theoretically with the UHF method. If a defect is localized and its interactions with the rest of the crystal are short-ranged, it can formally be represented by a periodic model, such as that adopted by the CRYSTAL program, provided that a suitable supercell can be found [73 to 75], i.e. a multiple of the unit cell, that is large enough to make the mutual interaction among neighbouring defects negligible, but still in the range of a computationally accessible problem. As far as the condition of non-interacting defects is satisfied, the method is fairly accurate and size consistent: the numerical accuracy of the implemented algorithms is such that the calculated energy per supercell of a crystal is precisely proportional to the supercell volume [74]. An analysis of the dependence of the formation energy (E_f) of $[Li]^0$ centres in MgO, for example, on the supercell size (see Table 1 in Ref. [76]) shows that big supercells may be necessary to compute E_f very accurately, but a supercell of 32 atoms (S_{32}) allows the calculation of

the defect formation energy within a few percent error and to account for the most important relaxation effects.

The UHF calculation provides very similar electronic structures for all these systems. The unpaired electron, that is formed after the substitution of an alkali metal ion for a cation in alkaline earth oxides, could in principle be found in two different electronic configurations:

– fractions of the unpaired electron almost symmetrically delocalized on the oxygen ions nearest neighbours of M^+;

– the M^+ ion coupled to one of the oxygen ions, forming a well localized electron hole.

UHF calculations lead to the localized electron hole solution unequivocally, in agreement with the experimental indications, and the localized configuration is preferred to the delocalized one by about 300 kJ/mol.

As examples, we refer to bulk $[Li]^0$ and $[Na]^0$ centres in CaO, calculated with the S_{64} supercell at the HF equilibrium geometry for CaO (lattice parameter: 4.83 Å; expt.: 4.79 Å). We refer to Refs. [76, 77] for technical details of the calculation. The band structure is particularly useful for the characterization of the defect. Figure 7 shows the valence and conduction bands of $[Li]^0$ in CaO, that are essentially due to the p-type oxygen orbitals. The levels corresponding to the p electrons of O^- are split from the valence band originated by the p atomic orbitals of the O^{2-} ions: the populated levels, i.e. the doubly degenerate p_x–p_y and the α-p_z levels (z along the ionic pair axis) move to lower energy values (α-p_z is stabilized for as much as -608 kJ/mol from the bottom of the O^{2-} p valence band), and a β-p_z level appears in the large band gap, due to the electron hole. This picture is supported by the atomic net charges of M^+ and O^- (O_1) reported in Table 2 and obtained from Mulliken population analysis, which are very close to ± 1 $|e|$. Also the spin moment of O_1 is very close to one, indicating that the unpaired electron is almost completely localized and only very small fractions of spin density are found on the neighbouring ions. A more detailed description of electron

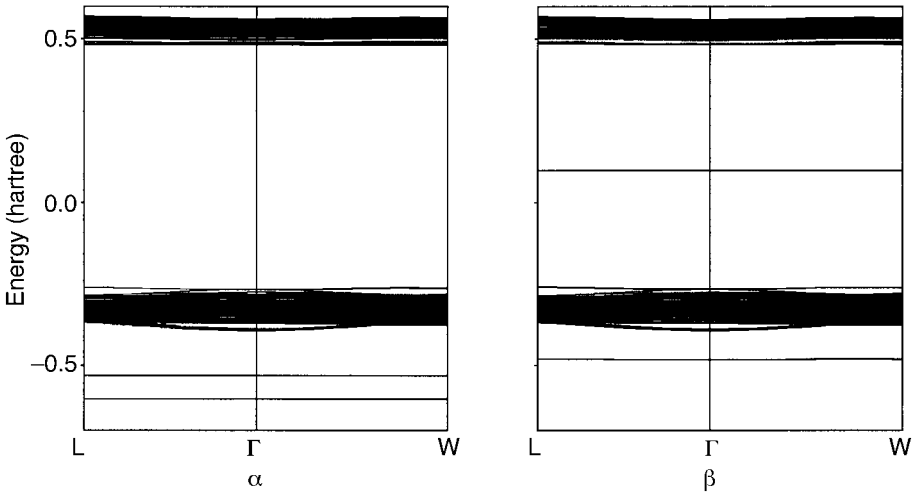

Fig. 7. Band structure of Li-doped CaO obtained with the S_{64} supercell for α- and β-spin states

Table 2
Net atomic charges (q) and spin moments (μ) evaluated according to a Mulliken partition of the periodic densities. Units: electrons. Labels of the atoms as in Fig. 8

	M		O_1		O_2	
	q	μ	q	μ	q	μ
$[Li]^0$ in CaO	0.980	0.000	−1.047	0.985	−1.932	0.002
$[Na]^0$ in CaO	0.998	−0.002	−1.053	0.986	−1.928	0.003

charge and spin density is given in Fig. 8 for a $[Li]^0$ centre in CaO. The unpaired electron is clearly localized on O_1 with some residual spin density spread in the region around the defect, oscillating from positive to negative values.

It results from energy minimization that the M^+ and O^- monovalent ions move in opposite directions and increase their mutual distance, R (Table 3), as they are less attracted by each other than by their neighbouring bivalent O^{2-} and Ca^{2+} ions. This is in reasonable agreement with the experimental indications, despite the rough approximations in the model used to derive R from primary experimental data [66, 71, 72]. The theoretical method allows us to distinguish the individual displacements of M and O_1 from their lattice positions: the M^+ ions are between 3 and 4 times more mobile than O^-. This increase in the $M–O_1$ distance with respect to the perfect lattice interionic distance (4.83 Å) is remarkable when M = Li. The higher mobility of the small Li^+ ion allows a stronger electrostatic interaction with the surrounding ions and corresponds to a higher relaxation energy, which is nearly three times as large as for Na. The displacements of the neighbouring oxygen ions from their lattice positions are not as large as for M, but the corresponding relaxation energies are far from negligible, especially for M = Na (31 kJ/mol), whereas it is less important for Li (5 kJ/mol).

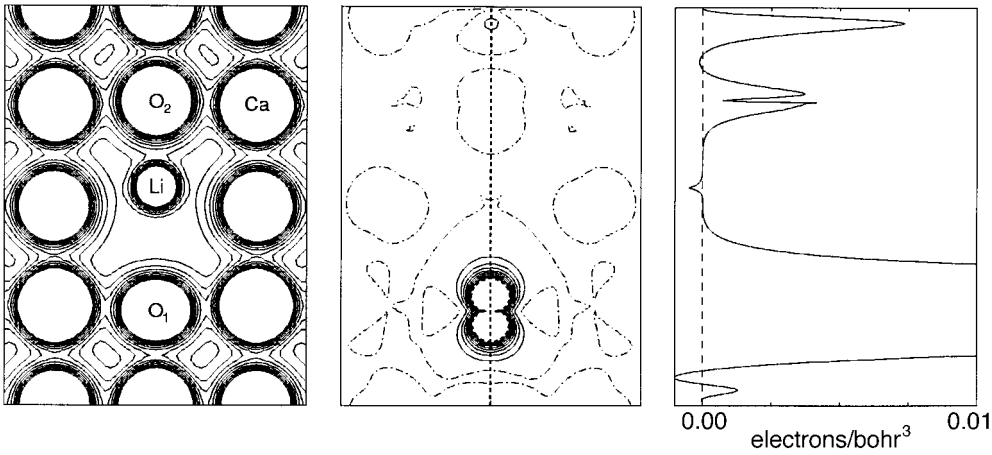

Fig. 8. Total electron charge (left) and spin (middle) density maps in the (100) plane through the $Li^+–O^-$ pair. On the right, the spin density function along the vertical path dashed in the spin map. The separation between contiguous iso-density curves in the maps corresponds to 0.01 e/Bohr^3 in the total charge density and 0.005 e/Bohr^3 in the spin map. Symbols as in Fig. 5

Table 3
Relaxation of M and O_1, and M–O_1 distances (R) in Å. The experimental values (R^{exp}) reported were obtained with different interpreting models

	Δz_M	Δz_O	R	R^{exp}
$CaO:[Li]^0$	0.44	−0.11	2.91	2.86−3.05[a]), 2.83 ± 0.19[b])
$CaO:[Na]^0$	0.25	−0.08	2.74	2.23 to 2.46[c])

[a]) Ref. [72]; [b]) Ref. [66]; [c]) Ref. [71].

A straight comparison between calculated and experimental data is possible for the parameters that determine the hyperfine structure of the spectra [72]: the hyperfine coupling constants a and b and the nuclear quadrupole coupling constant P. These constants appear in the formulation of the spin Hamiltonian in terms of which the ENDOR spectra are interpreted.

The isotropic (a) and anisotropic (b) hyperfine coupling constants (in MHz) are expressed for each nucleus N as [78]

$$a_N = \frac{2\mu_0}{3h}\, g\beta_e g_N \beta_n \varrho^{\alpha-\beta}(0)\,, \tag{43}$$

$$b_N = \frac{2\mu_0}{3h}\, g\beta_e g_N \beta_e \left[T_{11} - \frac{1}{2}\,(T_{22} + T_{33})\right], \tag{44}$$

where the spin density $\varrho^{\alpha-\beta}$ at N, the elements of the hyperfine coupling tensor $\mathbf{T}$ and the electron g factor are the only terms which depend on the electronic structure of the system (in our calculation we use the free electron g to approximate the true g factor, which is usually an acceptable approximation for our purpose). The other multiplicative factors in Eq. (43) and (44) are all tabulated constants [78, 79] (h, the Planck constant, β_e and β_n, the electronic and nuclear magnetons, μ_0, the permeability of the vacuum and g_N, the nuclear g factor). $\mathbf{T}$ is a tensor of rank two, that is obtained as the quadrupole moment of the spin density at N. Its generic element has the form:

$$T_{ij}^N = \sum_{\mu\nu}\sum_{\mathbf{G}} P_{\mu\nu\mathbf{G}}^{spin} \int \varphi_\mu(\mathbf{r}) \left(\frac{r^2\delta_{ij} - 3r_i r_j}{r^5}\right) \varphi_\nu(\mathbf{r} - \mathbf{G})\, d\mathbf{r}\,, \tag{45}$$

where the origin of the reference system is at nucleus N and r_i denotes the i-th component of r. T_{ii} in equation (44) are the elements of $\mathbf{T}$ in diagonal form, following the convention that T_{11} is the maximum module component.

The other important parameters in the spectrum are the nuclear quadrupole coupling constants P_N, that measure the coupling of the electric field gradient (q_N^{efg}) with the nuclear quadrupole moment (Q_N) at N,

$$P_N = \frac{3}{h}\,\frac{e^2 q_N^{efg} Q_N}{4I(2I-1)}\,, \tag{46}$$

where I is the total nuclear spin quantum number, e the electron charge magnitude, Q_N is measured experimentally and q_N^{efg} is obtained from a tensor of the same form as $\mathbf{T}$ where the spin density matrix in (45) is replaced by the total density matrix.

The calculated and experimental values of a, b and P for the coupling of the unpaired electron to the M nucleus in M-doped CaO are compared in Table 4. The best

Table 4
Spin Hamiltonian hyperfine isotropic (a) and anisotropic (b) coupling constants and nuclear quadrupole coupling constant (P) at nucleus M in doped CaO. Comparison between calculated (HF) and experimental [72] values. Units: MHz

	a		b		P	
M	calc.	exp.	calc.	exp.	calc.	exp.
Li	−0.819	−2.472	1.468	1.317	0.001	0.009
Na	−2.538	−9.145	1.558	1.877	0.449	0.446

agreement between the calculated and experimental results is obtained for b, with a percentage error within 15% of the experimental value. The same error range for b has been found also for MgO and SrO [77].

The calculated value of P_N is surprisingly good for CaO when N = Na, though it must be remarked that the variability of the values of Q reported by different authors is rather large and the calculation of P is obviously affected by the same uncertainty (data in Table 4 were obtained for $Q_{Li} = -0.03$ and $Q_{Na} = 0.14$ barn, as reported in the International Tables of Physics and Chemistry [79], Vol. 9, p. 31). In the Li case, both experimental and calculated P values are negligible.

As regards a, an accurate estimation is a more difficult task, since it requires a very precise determination of spin density at nuclei where it can be nearly zero. This is particularly true in this case, where the unpaired electron is very well localized on O^- and very low spin densities are found anywhere else in the crystal (see the spin moment values in Table 2. Nevertheless, it has already been emphasized that Fig. 8 reveals a well defined pattern for the residual spin density, with an alternation of positive and negative zones, that is not random; it is rather a consequence of spin polarization [80]: the electrons in the defect region with the same spin (α) as the unpaired electron, are stabilized by exchange and super-exchange interactions and, for this reason, they interact with it in a slightly more favourable way. Therefore, not only the absolute value of a is important, but also its sign, as it specifies if α- or β-spin electrons prevail at the nuclei. In Fig. 8 (right) the profile of spin density in CaO along the Li–O^- axis is shown in detail. What determines the value of a_{Li} is the depth of the small negative peak (about 5×10^{-4} $|e|$/Bohr^3) at Li, i.e. almost three orders of magnitude less than spin density at O_1 (O^-) and one order of magnitude less than that at O_2 (incidentally, the twin peak at O_2 implies p_z character, like for O_1). The agreement of the calculated a_N with the experimental data obtained from ENDOR spectra (Table 4) is only semi-quantitative, though the sign and the order of magnitude are correct, and the calculated a_N values scale approximately with the same trend as the experimental data, as can also be seen for MgO and SrO in Ref. [77]. From the computational point of view, particular caution is required to the level of convergence of the SCF cycle which is needed for a spin density of the order of 10^{-4} $|e|$/Bohr^3 to be determined with the necessary precision. Convergence of the order of 1×10^{-5} Hartree on total energy, which is adequate for the calculation of most observables, may be insufficient to evaluate a correctly, as is shown in Table 5 for Li-doped CaO. Attempts at improving the basis sets (either the valence or the core functions) and altering the geometry of the defect, as well as better approximating the Coulomb and exchange series or using a denser net in reciprocal

Table 5
Spin Hamiltonian hyperfine isotropic (a) and anisotropic (b) coupling constants and nuclear quadrupole coupling constant (P) at Li in doped CaO as a function of the level of convergence of the SCF cycle, when the precision in the calculation of total energy is 10^{-x} Hartree. Units: MHz

x	a_{Li}	b_{Li}	P_{Li}
5	−0.952	1.468	0.001
6	−0.920	1.468	0.001
7	−0.854	1.468	0.001
8	−0.819	1.468	0.001
9	−0.809	1.468	0.001
10	−0.807	1.468	0.001
11	−0.805	1.468	0.001
12	−0.805	1.468	0.001

space, do not lead to any significant improvement in the evaluation of a_N and the poor agreement between calculation and experiment is likely to be considered as a limit of the method: the spin densities involved are so low that the lack of electron correlation and the spin contamination intrinsic in the UHF approximation (the UHF wave function is an eigenfunction of the $\widehat{S}_z$ operator and not of the total spin momentum $\widehat{S}^2$) may be important.

In order to have some indications about the importance of electron correlation in the determination of a, a comparison with results obtained with DFT based Hamiltonians would have been useful. However, we did not succeed in localizing the electron hole onto one oxygen ion with DFT methods. In particular, the LSDA unpaired electron is nearly completely delocalized over the six oxygens around the defect, in contrast with the experimental evidence. This result seems to confirm the tendency of LSDA, already observed for NiO (Fig. 5), to delocalize unpaired electrons in tightly bound states onto neighbouring atoms. In the case of NiO, however, stoichiometry limits charge transfer from each Ni to a single O ion (the overall delocalization is about 25%), whereas, in the present case, six O ions are available and delocalization can proceed further.

5.3 F-centres in lithium fluoride

The capability of the method to reproduce the experimental values of b and P with a quite satisfactory accuracy and, at the same time, the difficulty in computing a as accurately as b and P have stimulated the investigation of other paramagnetic species, which are characterized by a stronger Fermi contact, such as F-centres in alkali halides, and for which very accurate ENDOR measurements [81] are available in the literature. Alkali halides are similar to alkali earth oxides as concerns crystal symmetry (same space group) and ionicity, and the F-centres offer the advantage of a simpler electronic structure than the electron holes in doped oxides.

As an example, we consider F-centres in lithium fluoride. The model is a 64 atom supercell crystal at the experimental lattice parameter, from which an F atom has been removed. The F-centre consists of an unpaired electron localized inside the vacancy, as can be seen in Fig. 9 and from the Mulliken population analysis (Table 6), but the picture differs from that of the trapped holes in alkaline earth oxides in some respects: the electron wave function in the vacancy has spherical symmetry and is much

more diffuse; relaxation of the nuclei surrounding the defect is negligible in this case (the Li ions around the vacancy are displaced by only 0.03 Å far from it, with an energy gain of just 1.7 kJ/mol). The unpaired electron in the vacancy is obviously more weakly bound than the electron of O^- in the trapped hole centre. A bound α-spin level appears in the valence–conduction band gap in this case, whereas the unpaired electron state of $[M]^0$ centres was stabilized below the O^{2-} p valence band. As in the previous examples, we compared HF with LDA results, using Dirac-Slater exchange potential [82] and the Perdew-Zunger parametrization of the Ceperley-Alder free electron gas correlation [83]. A discrete bound (α) and the corresponding unbound (β) levels appear in the gap also in the LSDA band structure, which is qualitatively similar, but differ from UHF quantitatively: the band gap is 936 kJ/mol (UHF: 2130 kJ/mol) and the energy difference between the defect α and β levels is 156 kJ/mol (UHF: 981 kJ/mol). This great difference in stability of the F-centre corresponds indeed to different electron charge and spin density distributions (Fig. 9). Mulliken analysis (Table 6) assigns almost exactly one electron to the UHF vacancy, while there are only 0.887 electrons in the LSDA vacancy. At the atoms around the defect, the spin moments calculated with both methods (Table 6) are nearly three orders of magnitude smaller than in the vacancy. Nevertheless, the spin density profiles in Fig. 9 show that the two sharp symmetric side peaks, which correspond to the Li nuclei, are about as high as the large middle peak centred at the vacancy. Since the heights of the Li peaks measure the spin density at those nuclei and the Fermi contact interaction at Li depends on it, the corre-

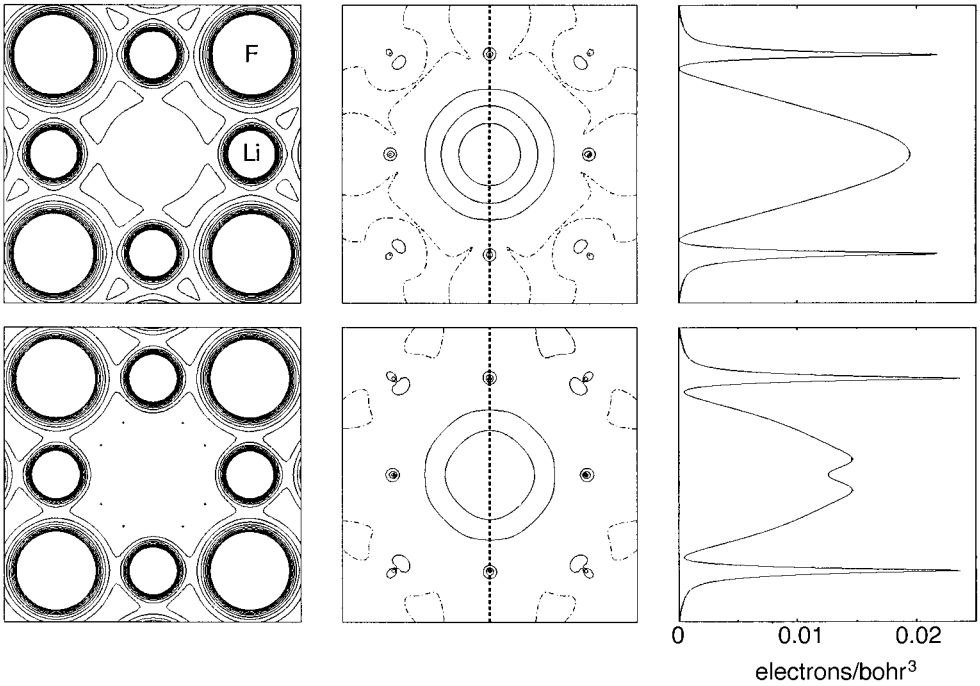

Fig. 9. HF (top) and LDA (bottom) total electron charge (left) and spin (middle) density maps in the (100) plane through the vacancy. On the right, the spin density function along the vertical path dashed in the spin map. Symbols and units as in Fig. 8

Table 6
Net atomic charges (q) and spin moments (μ) evaluated with the HF and LDA approximations according to a Mulliken partition of the periodic densities. Units: electrons. Labels of the atoms as in Fig. 9

	F-centre		Li		F	
	q	μ	q	μ	q	μ
HF	−1.002	1.085	0.978	0.003	−0.975	−0.009
LDA	−0.887	0.951	0.986	0.007	−0.961	0.001

Table 7
Spin Hamiltonian hyperfine isotropic (a) and anisotropic (b) coupling constants at first (Li) and second (F) nearest neighbours of the F-centre in LiF, as calculated in the HF and LDA approximations and measured experimentally with ENDOR spectroscopy [81]. Units: MHz

	Li		F	
	a	b	a	b
HF	38.571	3.244	76.375	11.257
LDA	41.811	3.150	105.56	13.720
expt.	39.0	3.2	105.9	14.9

sponding a constant value is large and positive. The same happens for the F ions around the vacancy. Table 7 shows that, in this case, where we deal with spin densities at the nuclei of the order of 10^{-2} $|e|$/Bohr^{-3} (two orders of magnitudes larger than in the trapped hole case) the agreement between the calculated and experimental values is satisfactory not only for b, but also for a, especially when the first nearest neighbours (Li) are involved. For farther neighbours of the vacancy the UHF error in a and b tends to increase (see Table 7 for the F ions), whereas the LSDA approximation seems to perform better. As a matter of fact, the tendency of LSDA to delocalize unpaired electrons, which prevents from describing well localized states (3d electrons in NiO and 2p electrons in $[M]^0$) correctly, is particularly suitable in the present case, where the unpaired electron occupies a very diffuse 1s state and leads to results in better agreement with experiment than UHF.

6. Conclusions

In this chapter we have recalled the fundamentals of the HF method and discussed how it can be used for the study of periodic structures. For the latter purpose we have made reference to a specific implementation, that embodied in the CRYSTAL public code. While this is not the most general possibility (in particular, the choice of using localized Gaussian functions to describe the crystalline orbitals pervades the very structure of the code and dictates many technical solutions), we have been able in this way to show concretely some of the subtleties which are needed to realize from the basic equations a powerful, efficient and useful tool.

Our second main objective has been to demonstrate through examples the usefulness of the HF method in solid state applications. In this sense we have been necessarily

confronted with DFT, the alternative approach which represents nowadays the favourite choice for the overwhelming majority of workers in this field of studies. In spite of all its merits, DFT is known to meet with serious difficulties in the description of systems with well localized spin densities which cannot be described through statistical local averages of exchange interactions. The examples here reported (which have been partly elaborated specially for the present work) are all concerned with this kind of problems. In our opinion, they prove convincingly the merits of the HF technique if not else as an auxiliary technique to DFT calculations.

There is, however, a more fundamental issue which justifies the effort towards the continuous improvement of HF-based techniques, and this comes from molecular quantum mechanics. At variance with DFT, standard quantum-chemical schemes can provide (in principle, at least) results of any required accuracy concerning ground and excited states of many-electron systems. In this respect, programs like CRYSTAL provide a unique opportunity to implement and test post-HF schemes for crystalline systems.

Acknowledgements The present work is part of a project coordinated by A. Zecchina and co-financed by the Italian MURST (Cofin98, Area 03). Financial support from the Italian C.N.R. is acknowledged.

References

[1] D.J. HEHRE, W.A. LATHAN, M.D. NEWTON, R. DITCHFIELD, and J.A. POPLE, GAUSSIAN70, Program number 236, QCPE, Indiana University, Bloomington (Indiana) 1970.
[2] V. FOCK, Z. Phys. **61**, 126 (1930).
[3] J.C. SLATER, Phys. Rev. **35**, 210 (1930).
[4] C.C.J. ROOTHAAN, Rev. Mod. Phys. **23**, 69 (1951).
[5] G.G. HALL, Proc. Roy. Soc. **A205**, 541 (1951).
[6] S.F. BOYS, Proc. Roy. Soc. **A200**, 542 (1950).
[7] S.F. BOYS, Proc. Roy. Soc. **A201**, 125 (1950).
[8] S.F. BOYS, G.B. COOK, C.M. REEVES, and I. SHAVITT, Nature (London) **178**, 1207 (1956).
[9] E. CLEMENTI and R. ROETTI, Atomic Data Nucl. Data Tables **14**, 177 (1974).
[10] S. HUZINAGA, Gaussian Basis Sets for Molecular Calculations, Elsevier Publ. Co., Amsterdam 1984.
[11] V. R. SAUNDERS, in: Computational Techniques in Quantum Chemistry and Molecular Physics, Eds. G.H.F. DIERCKSEN, B.T. SUTCLIFFE, and A. VEILLARD, Reidel, Dordrecht 1975 (p. 347).
[12] L.E. MCMURCHIE and E.R. DAVIDSON, J. Comput. Phys. **26**, 218 (1978).
[13] V. R. SAUNDERS, in: Methods in Computational Molecular Physics, Eds. G.H.F. DIERCKSEN and S. WILSON, Reidel, Dordrecht 1983 (p. 1).
[14] V.R. SAUNDERS and J.H. VANLENTHE, Mol. Phys. **48**, 923 (1983).
[15] M.F. GUEST and S. WILSON, Chem. Phys. Lett. **75**, 66 (1980).
[16] P. DEAK, in: Properties of Crystalline Silicon, Ed. R. HULL, EMIS Datareview Series, Vol. 20., INSPEC, London 1999 (p. 245).
[17] P. HOHENBERG and W. KOHN, Phys. Rev. **136**, B864 (1964).
[18] W. KOHN and L.J. SHAM, Phys. Rev. **140**, A1133 (1965).
[19] M.J. FRISCH, G.W. TRUCKS, H.B. SCHLEGEL, P.M.W. GILL, B.G. JOHNSON, M.A. ROBB, J.R. CHEESEMAN, T.A. KEITH, G.A. PETERSON, J.A. MONTGOMERY, K. RAGHAVACHARI, M.A. AL-LAHAM, V.G. ZAKRZEWSKI, J.V. ORTIZ, J.B. FORESMAN, J. CIOLOWSKI, B.B. STEFANOV, A. NANAYAKKARA, M. CHALLACOMBE, C.Y. PENG, P.Y. AYALA, W. CHEN, M.W. WONG, J.L. ANDRES, E.S. REPLOGE, R. GOMPERTS, R.L. MARTIN, D.J. FOX, J.S. BINKLEY, D.J. DEFREES, J. BAKER, J.P. STEWART, M. HEAD-GORDON, C. GONZALEZ, and J.A. POPLE, GAUSSIAN94, revision C.3, Gaussian, Inc., Pittsburg (P.A.) 1995.
[20] R. DOVESI, C. PISANI, C. ROETTI, M. CAUSÀ, and V.R. SAUNDERS, CRYSTAL 88 Program number 577, QCPE, Indiana University, Bloomington (Indiana) 1989.
[21] H. PREUSS, Z. Naturf. **11a**, 823 (1956).

[22] C.A. Weatherford and H.W. Jones (Eds.), ETO Multicenter Molecular Integrals, Reidel, Dordrecht 1982.
[23] V. R. Saunders, R. Dovesi, C. Roetti, M. Causà, N.M. Harrison, R. Orlando, and C.M. Zicovich-Wilson, Crystal98, User's Manual, Università di Torino, Torino 1998.
[24] C. Pisani, R. Dovesi, and C. Roetti, Hartree-Fock ab initio Treatment of Crystalline Systems, Lecture Notes Chem., Vol. 48, Springer-Verlag, Berlin 1988.
[25] R. McWeeny, Proc. Phys. Soc. (London) **74**, 385 (1959).
[26] J.M. André, L. Gouverneur, and G. Leroy, Internat. J. Quantum Chem. **1**, 451 (1967).
J.L. Brédas, J.M. André, J.G. Fripiat, and J. Delhalle, Gazz. Chim. Ital. **108**, 307 (1978).
[27] G. Del Re, J. Ladik, and G. Biczó, Phys. Rev. **155**, 997 (1967).
[28] A. Karpfen, Internat. J. Quantum Chem. **19**, 1207 (1981).
[29] A.B. Kunz, Phys. Rev. B **6**, 606 (1972).
[30] R.N. Euwema, D.L. Wilhite, and G.T. Surratt, Phys. Rev. B **7**, 818 (1973).
[31] V.R. Saunders, C. Freyria-Fava, R. Dovesi, L. Salasco, and C. Roetti, Mol. Phys. **77**, 629 (1992).
[32] R. Dovesi, in: Quantum-Mechanical ab initio Calculation of the Properties of Crystalline Materials, Ed. C. Pisani, Lecture Notes Chem., Vol. 67, Springer-Verlag, Berlin 1996 (p. 179).
[33] M. Catti, G. Valerio, R. Dovesi, and M. Causà, Phys. Rev. B **49**, 14179 (1994).
[34] M. Catti, F. Freyria Fava, C. Zicovich, and R. Dovesi, Phys. Chem. Minerals **26**, 389 (1999).
[35] M.D. Towler, R. Dovesi, and V.R. Saunders, Phys. Rev. B **52**, 10150 (1995).
[36] M. Catti and G. Sandrone, Faraday Discuss. **106**, 189 (1997).
[37] R. Dovesi, F. Freyria Fava, C. Roetti, and V.R. Saunders, Faraday Discuss. **106**, 173 (1997).
[38] R. McWeeny, Proc. Roy. Soc. (London) **A241**, 239 (1957).
[39] I.H. Hillier and V.R. Saunders, Internat. J. Quantum Chem. **4**, 503 (1970).
[40] J.A Pople and R.K. Nesbet, J. Chem. Phys. **22**, 571 (1954).
[41] R. Dovesi, V. R. Saunders, and C. Roetti, Crystal92, User's Manual, Università di Torino, Torino 1993.
[42] R. Dovesi, V. R. Saunders, C. Roetti, M. Causà, N.M. Harrison, R. Orlando, and E. Aprà, Crystal95, User's Manual, Università di Torino, Torino 1996.
[43] A.D. Becke, Phys. Rev. A **38**, 3098 (1988).
[44] C. Lee, W. Yang, and R.G. Parr, Phys. Rev. B **37**, 785 (1988).
[45] A.D. Becke, J. Chem. Phys. **98**, 5648 (1993).
[46] M.D. Towler, A. Zupan, and M. Causà, Comp. Phys. Commun. **98**, 181 (1996).
[47] A.D. Becke, J. Chem. Phys. **88**, 2547 (1988).
[48] R. Dovesi, C. Pisani, C. Roetti, and V.R. Saunders, Phys. Rev. B **28**, 5781 (1983).
[49] D. Moncrieff and V.R. Saunders, Doc NAT648, University of Manchester Regional Computing Center, 1986.
[50] V.R. Saunders, C. Freyria-Fava, R. Dovesi, and C. Roetti, Comp. Phys. Commun. **84**, 156 (1993).
[51] M. Causà, R. Dovesi, R. Orlando, C. Pisani, and V.R. Saunders, J. Phys. Chem. **92**, 909 (1988).
[52] R. Dovesi, Internat. J. Quantum Chem. **29**, 1755 (1986).
[53] M. Lax, Symmetry Principles in Solid State and Molecular Physics, John Wiley & Sons, New York 1974.
[54] C.M. Zicovich-Wilson and R. Dovesi, Internat. J. Quantum Chem. **67**, 299 (1998).
[55] C.M. Zicovich-Wilson and R. Dovesi, Internat. J. Quantum Chem. **67**, 311 (1998).
[56] C.M. Zicovich-Wilson and R. Dovesi, Chem. Phys. Lett. **277**, 227 (1997).
[57] R. Dovesi, C. Pisani, F. Ricca, and C. Roetti, Phys. Rev. B **22**, 5963 (1980).
[58] R. Dovesi, C. Pisani, and C. Roetti, Internat. J. Quantum Chem. **17**, 517 (1980).
[59] T. Oguchi, K. Terakura, and A.R. Williams, Phys. Rev. B **28**, 6443 (1983).
[60] K. Terakura, T. Oguchi, A.R. Williams, and J. Kübler, Phys. Rev. B **30**, 4734 (1984).
[61] A. Svane and O. Gunnarson, Phys. Rev. Lett. **65**, 1148 (1990).
[62] S. Massida, M. Posternak, and A. Baldereschi, Phys. Rev. B **46**, 11705 (1992).
[63] W.C. Mackrodt, N.M. Harrison, V.R. Saunders, N.L.Allan, M.D. Towler, E. Aprà, and R. Dovesi, Phil. Mag. **68**, 653 (1993).
[64] M.D. Towler, N.L. Allan, N.M. Harrison, V.R. Saunders, W.C. Mackrodt, and E. Aprà, Phys. Rev. B **50**, 5041 (1994).
[65] G. Rius, R. Cox, R. Picard, and C. Santier, C.R. Acad. Sci. (France) **271**, 824 (1970).

[66] O.F. Schirmer, J. Phys. Chem. Solids **32**, 499 (1971).
[67] H.T. Tohver, B. Henderson, Y. Chen, and M.M. Abraham, Phys. Rev. B **5**, 3276 (1972).
[68] M.M. Abraham, Y. Chen, J.L. Kolopus, and H.T. Tohver, Phys. Rev. B **5**, 4945 (1972).
[69] D.J. Driscoll and J.H. Lunsford, J. Phys. Chem. **89**, 4415 (1985).
[70] T. Ito, J. Wang, C.H. Lin, and J.H. Lunsford, J. Amer. Chem. Soc. **107**, 5062 (1985).
[71] G. Rius and A. Hervé, Solid State Commun. **15**, 399 (1974).
[72] M.M. Abraham, W.P. Unruh, and Y. Chen, Phys. Rev. B **10**, 3540 (1974).
[73] C. Freyria-Fava, R. Dovesi, V.R. Saunders, M. Leslie, and C. Roetti, J. Phys.: Condensed Matter **5**, 4793 (1993).
[74] R. Orlando, R. Dovesi, P. Azavant, N.M. Harrison, and V.R. Saunders, J. Phys.: Condensed Matter **6**, 8573 (1994).
[75] R. Orlando, P. Azavant, M.D. Towler, R. Dovesi, and C. Roetti, J. Phys.: Condensed Matter **8**, 1123 (1996).
[76] A. Lichanot, C. Larrieu, R. Orlando, and R. Dovesi, J. Phys. Chem. Solids **59**, 7 (1998).
[77] A. Lichanot, C. Larrieu, C. Zicovich-Wilson, C. Roetti, R. Orlando, and R. Dovesi, J. Phys. Chem. Solids **59**, 1119 (1998); *Erratum:* J. Phys. Chem. Solids **60**, 855 (1999).
[78] J.A. Weil, J.R. Bolton, and E. Wertz, Electron Paramagnetic Resonance – Elementary Theory and Practical Applications, John Wiley & Sons, New York 1994.
[79] D.R. Lide (Ed.), Handbook of Chemistry and Physics, 72nd ed., CRC Press, Boca Raton 1991/1992.
[80] O.F. Schirmer, J. Phys. C **6**, 300 (1973).
[81] B. Henderson, Defects in Crystalline Solids, Edward Arnold, Ltd., London 1972.
[82] P.A.M. Dirac, Proc. Cambridge Phil. Soc. **26**, 376 (1930).
[83] J.P. Perdew and A. Zunger, Phys. Rev. B **23**, 5048 (1981).